Analytical and Bioanalytical Chemistry
https://doi.org/10.1007/s00216-020-02579-8

RESEARCH PAPER

Design of a DOPC-MoS_2/AuNP hybrid as an organic bed with higher amplification for miR detection in electrochemical biosensors

Mohammad Kaji Yazdi[1] · E. Ghazizadeh[2] · Mahya Noroozi[3] · Ali Neshastehriz[4,5]

Received: 20 January 2020 / Revised: 26 February 2020 / Accepted: 4 March 2020

Abstract

The liposome-based biosensors are used for detection of nucleic acids and proteins as organic beds which are biocompatible tools for point of care tests, but their lack of sensitivity has been challenging. Therefore, designing a proper strategy is vital to increase the sensitivity of the target in diagnostic tests. In this study, for the first time, we use a combination of cationic DOPC liposome (dioleoylphosphatidylcholine) with MoS_2 to enhance the sensitivity of liposomal sensors clearly. The electrochemical measurements are performed between potentials at − 0.4 V and + 0.4 V with 1 mM $[Fe(CN)_6]^{-3/-4}$. At first, we construct the DOPC/MoS_2 hybrid (as a mineral/organic bed) to promote higher electrochemical behavior than DOPC liposome (as organic bed). In this research, adding AuNP can cause attachment with both the DOPC and MoS_2. Therefore, the electrochemical reactions are enhanced accordingly to provide more positions for attaching the probes on the AuNP. So our DOPC-MoS_2/AuNP hybrid can detect miR-21 with high sensitivity (LOD = 10 aM) because of attachment of miR-21 to MoS_2/AuNP in addition to DOPC/AuNP. This sensor has also high specificity and repeatability as a biocompatible sensor, which can be used in point of care tests and transduction instruments.

Keywords Liposome · Biosensor · MicroRNA · Point of care

Introduction

Circulating microRNAs are fragments of single-stranded non-coding RNA (ncRNA) of 19–25 nucleotides which have various functions in the cellular pathways [1, 2]. Recent evidence suggests that microRNAs (miRNAs) acted as a "mediator" that regulates numerous targets [3]. Having the same function in the intracellular and intercellular pathways made them as biomarkers for cancer diagnosis in body fluids such as the serum and blood [4]. The use of sensitive methods to detect miRs has been necessary due to their small size and low concentration [5]. Most standard methods have challenges such as low repeatability method errors and the complexity of the protocol [6]. Recently, extensive studies have been developed to detect miRs using biosensors [7, 8]. Electrochemical biosensors are more reliable than optics because they do not use probes and labeling [9]. Recently, papers about biocompatibility biomaterial on the developments in the electrochemical sensors were reported [10, 11]. Various types of liposomal surfaces to detect miRs as an electrochemical amplifier have been used. Various combinations of liposomes as dioleoylphosphatidylethanolamine (DOPE) and 1,2-dioleoyl-

Electronic supplementary material The online version of this article (https://doi.org/10.1007/s00216-020-02579-8) contains supplementary material, which is available to authorized users.

✉ E. Ghazizadeh
elhamgenetic@gmail.com

[1] Department of Pediatric Hematologist and Oncologist, Bahrami Children Hospital, Tehran University of Medical Sciences, Tehran 25529, Iran

[2] Department of Medical Biotechnology, School of Medicine, Mashhad University of Medical Sciences, Mashhad 25529, Iran

[3] Department of Plasma, Optic and Laser Center, Azad University, Tehran 25529, Iran

[4] Radiation Biology Research Center, Iran University of Medical Sciences (IUMS), Tehran 25529, Iran

[5] Radiation Sciences Department, Iran University of Medical Sciences (IUMS), Tehran 25529, Iran

Published online: 28 March 2020

3-trimethylammoniumpropane (DOTAP) in these applications have been reported [12, 13]. The spherical structure of these nanomaterials in tacking the more targets provides a proper bed for the electrochemical reactions [14]. The inability to have high sensitivity in detecting targets is an important challenge in the liposome-based biosensor [15]. As a result, designing the strategies to upgrade these biosensors is necessary [16, 17]. DOPC liposome is one of the liposomes, which has high biocompatibility features with weak bands. So, it attracted the attention of many researchers in electrochemical application [18]. On the other hand, MoS_2-based electrochemical sensors have the unique atomic structure that allows an easy intercalation with metal atoms or ions. But, this sensor has the inability performance due to the poor intrinsic conductivity [19]. Recent study showed that MoS_2 can connect to DOPC based on the van der Waals force interactions in drug delivery applications [20]. For the first time, we use the liposome-MoS_2 hybrid as a model for sensing miR-21 to prompt the sensitivity of liposomal sensor. Another material which we use in designing sensor is AuNP. There were the remarkable physicochemical properties of gold nanoparticles in the developments of biomolecular interactions with AuNP-containing sensors, in particular for microRNA detection due to improving sensitivity with increased surface area [21, 22]. On the other hand, the effect of AuNPs on the MoS2 nanosheets has been proved in the increased surface area for detection of targets and increased the sensitivity of the sensor [23]. After the construction of the DOPC-MoS_2 hybrid was made, AuNP was added to the modified surface to attach with thiolated probe which would be added then. Our research shows that AuNP not only can attach with MoS_2 but also can attach with DOPC by increasing the resistance due to more exchanges of the electrochemical reactions with creation of more sites to attach the probe and miR-21. So, we designed the novel DOPC-MoS_2/AuNP hybrid which it was composed MoS_2 and AuNP with improving the sensitivity of liposomal sensor to detect miR-21 (as the case of miR in the most diseases and cancers). We also proved that the electrochemical changes of the composition of the liposome with a nanomaterial (MoS_2) and AuNP on the solid surfaces.

Materials and methods

Materials

MoS_2 powder (10–30 m) from Chemical Aria Company (Tehran, Iran) was prepared. All of the reagents and chemicals were of analytical grade without further purification which were provided by Chemical Aria Co (Tehran, Iran). Electrochemical impedance spectroscopy (EIS) and differential pulse voltammetry (DPV) were used by SP-300 Instruments (SP-300) (Texas, USA). SCPE-GNP (screen carbon-printed electrode-gold nanoparticle) was functioned on the ceramic substrate (L 34 mm × W 10 mm × H 0.5 mm) from Drop Sens Inc. (Oviedo, Spain). It is consisted of a gold nanoparticle-carbon working electrode, a carbon counter electrode, and a silver reference electrode. DPV measurements were performed in the presence of 1 mM $[Fe(CN)_6]^{-3/-4}$ in PBS in the potential window − 0.4 V to + 0.4 V at a scan rate 50 mV s^{-1}. The frequency of impedance measurement ranged from 100 kHz to 1 Hz of $[Fe(CN)_6]^{-3/-4}$ in PBS pH = 7.4. We used ZSimpWin 3.22 (Princeton Applied Research) to analyze the EIS spectra, and the data were presented in Nyquist plots. Non-contact of AFM images mode was acquired using Educational AFM from Bim Gostar Co. (Tehran, Iran). TEM images were done using TecnaiG2 20 instruments of FEI Company (Hillsboro, USA). Particle sizes and zeta potentials were used from Horiba nanoparticle size analyzer, Malvern Nano SZ-100, which uses green laser light at wavelength 532 nm. Analytical grade potassium ferrocyanide, potassium ferricyanide, sulfuric acid, sodium chloride, and potassium chloride were purchased from Chemical Aria (Tehran, Iran). 1,2-Dioleoyl-sn-glycero-3-phosphoethanolamine (DOPE) and 1,2-dioleoyl-sn-glycero-3-phosphocholine(DOPC) was procured from Sigma-Aldrich (USA). Deionized water (DI) was used for preparing all experimental solutions and hydrogen tetrachloroaurate (III) was prepared from Alfa Aesar. Thiolated oligonucleotides as probe: 5p′-ACAACAUCAGUCUGAUAAGCUA-HS -3′ and miR-21: 5′-UAG CUUAUCAGACUGAUGUUGA -3′ (RNA), non-complementary: 5′- GTA GACAAGCATGACGTACCTG -3′ (DNA) (control II), and single base mismatch (underlined): 5′-UAC CUUAUCACACUCAUCUUGA -3′ (RNA) (control III) were synthesized by MW GE Biotech, Ebersberg, Germany, without any purification.

Fabrication the DOPC-MoS_2/AuNP hybrid in GNP-SCPE for sensing miR-21

In this research, we used as DOPC-MoS_2 hybrid as an amplifier bed. At first, DOPC liposome was prepared by dissolving in chloroform at the ratio1:3, dried, rehydrated with buffer (pH = 7.4), and sonicated for 15 min and kept at 4 °C until use [24]. On the other hand, for providing the initial concentration of 50 mg/mL of MoS_2, its powder was added to deionized water. The obtained slurry was set overnight. Then the supernatant was collected and mixed with. DOPC liposome (50 μg 11 mL^{-1}) was mixed with various concentrations of MoS_2 (10, 25, 50, 100, 200, 300, 400, and 500 μg mL^{-1}) in buffer A for 20 min [25]. This mixture was centrifuged at 10,000 rpm for 10 min to precipitate. The 20 mL of prepared DOPC/MoS_2 gave the highest electrochemical response at 1:1 ratio and sonicated for 15 min to form DOPC/MoS_2 hybrids in solution. 1.2 μL of this mixture was dropped on the surface and stored at 4 °C for 1 h. The electrode was dried and carefully rinsed with water, dried again at room temperature, and

then used for the electrochemical test. To connect the probe on the modified surface, we used of the gold nanoparticles to connection with the liposome and the MoS_2. The gold nanoparticles were made by the citrate reduction method [26]. Dropping AuNP was done in two steps: first, 1 μM of AuNP solution was added on the MoS_2-DOPC hybrid to form covalence bond with DOPC and stored at 4 °C for 1 h. Then, AuNP decorated on MoS_2 nanosheets were synthesized by microwave-assisted one-pot method. Ten milliliters (23 μg mL^{-1}) of MoS_2 nanosheet aqueous dispersion was added into a 20-mL quartz tube equipped with a magnetic bar. One hundred twenty microliters TC (100 mmol L^{-1}), 20 μL Tween-80 (100 mmol L^{-1}), and 100 μL HAuCl4·$3H_2O$ (28.5 mmol L^{-1}) were stirred and mixed with MoS_2 nanosheet solution and heated to 60 °C for 5 min in a microwave reactor. Then, the mixture was stirred for 3 h at room temperature. Finally, the AuNP-MoS_2 nanocomposites were centrifuged (20 min, 7000 rpm) to remove excess reagents, the supernatant was discarded, and the precipitate was dispersed in ultrapure water [27].

Immobilization of RNA probe/miR-21 on the DOPC-MoS_2/AuNP/SCPE-GNP

The DOPC-MoS2/AuNP was utilized for electrochemical measurements. The electrode surface was initially cleaned by sonication in acetone and 2-propanol for 5 min in each solvent and dried under a stream of nitrogen. So, we added the thiolated probe (capture probe, 1 mM of 2 mL RNA in 1 M NaCl, pH = 7.0) to dropping of DOPC-MoS_2-AuNP hybrid in the individual electrodes and left for at 4 °C. The surfaces were washed with a blank buffer to remove the non-reacted probes. At the end, 1 μM of 2 mL (miR-21) were hybridized on the MoS_2-DOPC-AuNP surfaces for 4 h. Finally, the electrochemical measurements were performed between the potentials at + 0. 4 V and − 0.4 V in PBS.

Evaluation the specificity tests for sandwiched DOPC-MoS_2/AuNP for sensing miR-21 on the SCPE-GNP

To assess the specificity of the sandwiched sensor, three electrodes were incubated with 1 μM of 2 mL probe (for detection of miR-21) with 1 μM of the DNA and mismatch RNA, and one electrode was used as bare electrode which was incubated in the buffer for 24 h at 4 °C. In previous studies, AuNP with liposomes were used to enhance electrochemical reactions [26]. So in this research, not only the effect of MoS_2 on increase the electrochemical reactions was evaluated related to AuNP alone but also the differentiation of the electrochemical behavior of MoS_2 with DOPC relative to another cationic dioleoylphosphatidylethanolamine liposome (DOPE) were measured. DPV tests in the presence of DOPC/AuNP, DOPC/MoS_2, DOPE liposome/AuNP, DOPE/MoS_2 hybrids in the separate electrodes under identical conditions are recorded. The gold nanoparticles were made by the citrate reduction [22]. DOPC and DOPE liposomes were prepared by dissolving in chloroform at the ratio1:3, dried, rehydrated with buffer (pH = 7.4), and sonicated for 15 min and kept at 4 °C until use. To provide a concentration of 50 mg/mL of MoS_2, its powder was added to deionized water. Thus, prepared DOPE and DOPC liposomes were individually mixed with AuNP and MoS_2 solutions at 1:1 ratio and sonicated for 15 min to form liposome-AuNP or liposome-MoS_2 hybrids in the solution. Therefore, 1.2 mL of these hybrids were dropped on the surface and stored at 4 °C for 1 h. Then, the electrochemical tests had been done on separate electrodes.

Identification the sensitivity tests for sandwiched DOPC-MoS_2/AuNP for sensing miR-21

Prior to titration experiments, aliquots containing different concentrations of the miR-21 (1 aM to 100 fM) in 30 μL of the incubation buffer were prepared and were incubated with their probes on the DOPC-MoS_2/AuNP on the GNPs-SCP at 37 °C for 1 h in a dark humidity chamber. After washing with deionized nuclease-free water, DPV test was performed at each concentration of miR-21. In order to determine the effect of MoS_2 to increase the ability of detection of miRs, we used DOPC-AuNP modified as control test in another sensor. So the DOPC-AuNP hybrid was prepared in two steps: DOPC liposome was first prepared by dissolving in chloroform at the ratio1:3, dried, rehydrated with buffer (pH = 7.4) and sonicated for 15 min, and kept at 4 °C until use. Gold nanoparticles were made using by the citrate reduction [26]. In this stage, we prepare to titration experiments, aliquots containing different concentrations of the miR-21 (1 fM to 100 pM) in 30 μL of the incubation buffer were prepared that they were incubated with their probes on the DOPC-AuNP/SCPE-GNPs at 37 °C for 1 h in a dark humidity chamber. Then, the electrochemical tests have been investigated of these electrodes on the separate electrodes and the results were compared to DOPC-MoS2 as hybrid material in this study.

Detection of the stability and reproducibility for DOPC-Mos_2/AuNP/probe + miR-21 sensor on the SCPE-GNP

In order to investigate the effect of the MoS_2 in the stability and reproducibility of the liposomal sensors, the stability and reproducibility tests of DOPC-MoS_2/AuNP sensors were done. The stability of this sensor was measured on one electrode for 25 cycles and DPV changes of the electrochemical behaviors were examined for the separate electrode. Then we have simultaneously used five electrodes for detection of reproducibility of the DOPC-MoS_2/AuNP sensor. So, we started

to sandwich the different layers and reported the change of electrochemical behavior when the sensing of miR-21 was done for every electrode.

Results and discussion

Electrochemical characteristics of sandwiched DOPC-MoS_2-AuNP/probe

The differential pulse voltammetry of the modified GNP-SCPE electrode was sequentially measured with the electrodeposited of the DOPC-MoS_2-AuNP hybrid in the presence of 1 mM $[Fe(CN)_6]^{-3/-4}$ (Fig. 1). In this study, we used as PC (phosphatidylcholine) lipids, because they are highly biocompatible and the head group of lipids contains a negatively charged phosphate and a positive charge can be prepared in high surface area [28]. So, the increased electrochemical behavior of DOPC (as a control surface with PC group) confirms the high surface area in the electrode. So, the peak currents decreased from 10.1 to 9.8 μA as compared to the bare gold electrode with ΔE (Epa − Epc) 72 mV. Lui and his team showed that the hybrid material by WS_2 and DOPC liposomes could be formed with a stable adsorption complex likely via van der Waals forces as they deduced from washing the complex by various denaturing agents [21]. Therefore, in this research, we use DOPC-MoS2 hybrid in designing the sensor materials. Attachment of the DOPC-MoS_2 by dropping the casting on the GNP-SCPE caused the unchanged ΔEp and the peak current decreased from 9.8 to 7.9 μA. The electrochemical behavior of the sensor further through electrochemical impedance spectroscopy (EIS) was examined which was a good method for the characteristic of surface-modified electrodes. The model described this sensor is $R(C\ (RW))$, in which the semicircle diameter is equivalent to electron transfer resistance R_{et}, which limits the electron transfer kinetics of the redox probe at the interface of the electrode [23]. The R_{CT} value increased from 5.32×10^3 to 6.79×10^3 O cm^{-2} (Fig. 1B). The increase in the R_{CT} showed the enhanced performance of the biosensor due to the high conductivity of DOPC-MoS_2 hybrid and large surface-to-volume ratio of DOPC liposome. Our study showed that the attachment of the MoS_2 with DOPC liposomal sensor has a significant effect on the electrochemical behavior of DOPC-MoS_2 hybrid. The interactions of the MoS_2 group with DOPC may probably cause more surfaces to volume ratio and more cover of the pores in the liposomal surface that they can provide the more electrochemical exchanges with $[Fe(CN)_6]^{-3/-4}$ probe. The previous studies showed that the liposomal sensor has a good performance as the organic bed in the electrochemical changes. But their spherical structure limits the high detection of a target in the clinical test [28–30]. In the current study, the two-dimensional MoS_2 structure has probably provided the appropriate surface to upgrade the performance of the liposomal sensor. Afterwards, AuNP were used to connect the thiolate probe that they will be added later. Attachment of AuNP by dropping the casting on the DOPC-MoS_2 hybrid caused the peak current drastically reduced from 7.9 to 6.1 μA and R_{CT} value increased from 6.79×10^3 to 7.52×10^3 O cm^{-2} (Fig. 1A, B). The effect of the electrochemical reactions of AuNP has been confirmed by the increase in the charge exchange reactions with the $[Fe(CN)_6]^{-3/-4}$ probe on the different types of liposomes (DOPE, DOTAB) [29, 30]. On the other hand, the connected of AuNP with MoS_2 was proved to increase of electrochemical sensor [25, 26]. Therefore, we show that the intensity of electrochemical reactions could be due to the direct attachment of the AuNP with MoS_2, in addition to attachment of DOPC when it was added on the DOPC-MoS_2 hybrid on the sensor. These results provide more electrochemical exchange sites of AuNP in MoS_2 and DOPC beds

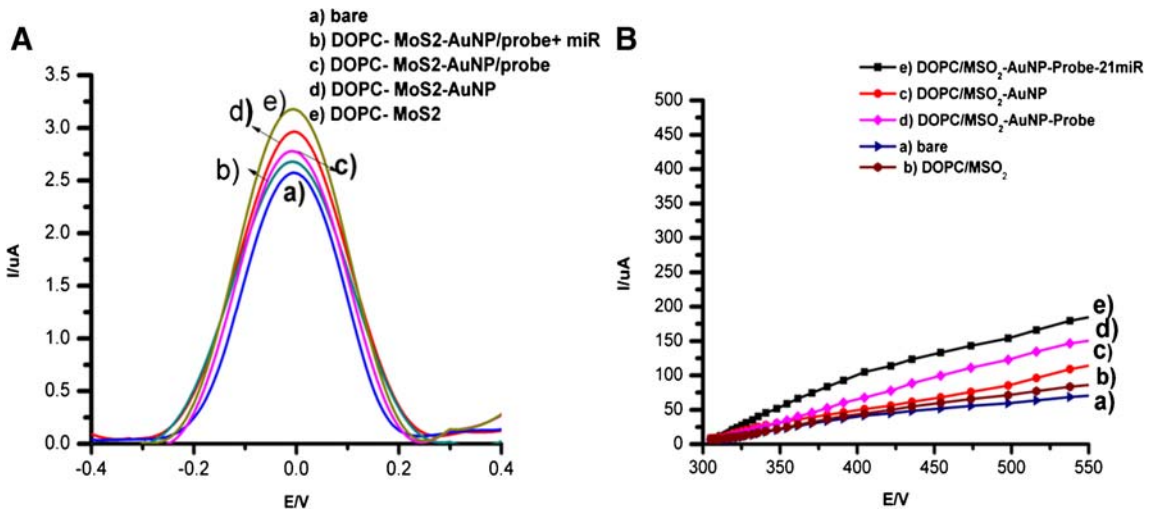

Fig. 1 **A** DPV and **B** EIS of behavior of the stages of DOPC-MoS_2-AuNP/probe + miR-21 sensor for sensing miR-21. Modified surfaces recorded at a scan rate 50 mV s^{-1} in phosphate buffer (pH 7.4) containing 1 mM $[Fe(CN)_6]^{-3/-4}$

in which they create more binding sites to attach probe and enhance the diagnostic sensitivity of miR-21.

Electrochemical behavior in detection of the mechanism of sensing miR-21

RNA sensing mechanism can be explained by hindering the electron transfer of the redox probe $[Fe(CN)_6]^{-3/-4}$ to the electrode surface when probe + miR-21 were formed as the following: adding probe 21 to the DOPC-MoS_2-AuNP hybrid caused to connect the AuNP, which was attached to the MoS_2 and DOPC. At this point, R_{CT} has continued increase more to 9.11×10^3 O cm^{-2} due to a more increase in negative charge density at the electrode/electrolyte interface by the presence of the complex nucleic acid probes with the $[Fe(CN)_6]^{-3/-4}$ probe in response to the electrostatic repulsion of MoS_2 and DOPC (Fig. 1A). At end, the addition of the miR-21 to the sensor caused the decrease of peak currents, too (Ipa was decreased from 5.1 to 4.4 μA) and the R_{CT} value increased from 9.11×10^3 to 10.14×10^3 O cm^{-2}. Charge density at the electrode/electrolyte interface by the presence of miR-21 with the $[Fe(CN)_6]^{-3/-4}$ probe in response to the electrostatic repulsion caused to higher R_{CT} than DOPC-MoS_2/AuNP modified with probe. Different steps about the formation of the modified sensor are shown in Fig. 2. So, we designed the simple DOPC-MoS_2/ AuNP hybrid with the stable adsorption of MoS_2 with DOPC complex which can occur via van der Waal forces. The mechanism of sensing miR-21 can explain the large surfaces of MoS_2 that enhances more electrochemical sites for AuNPs contributing to accelerated electron transfer between duplexes of miR-21 and $[Fe(CN)_6]^{-3/-4}$ probe and SCPE-GNP electrodes. In this study, we investigated the electron transfer rate constant (ks) of miR-21. So, the effect of the scan rate on the cyclic voltammetric performance of the DOPC-MoS_2/AuNP is calculated. Results show that the cathodic and anodic peak currents increased for the DOPC-MoS_2/AuNP linearly along with the scan rate in the range of 10~300 mV s^{-1} (see Electronic Supplementary Material (ESM) Fig. S1a). It can suggest that the electron transfer between miR-21 and SCPE-GNP electrode could be easily performed at the DOPC-MoS_2/AuNP hybrid and it was a surface-controlled process (ESM Fig. S2a). Based on the dependence of the peak separation (ΔEp) on scan rates, we estimated that the apparent electron transfer rate constant (ks) of miR-21 was 2.21 s^{-1}, which is smaller than that in DOTAB/AuNP bed (4.9 s^{-1}) [29] and DOPE-DOTAB/AuNP (5.32 ± 0.16 s^{-1}) [30]. Our results proved that DOPC-MoS_2/AuNP nanocomposite facilitates the electron transfer between the redox-active miR and the electrode.

Characterization of the surface of DOPC-MoS_2-AuNP/probe + miR on the GNP-SCPE

We used atomic force microscopy and transmission electron microscopy analysis to characterize the components of DOPC-MoS_2-AuNP/probe + miR-21. A typical layer-like

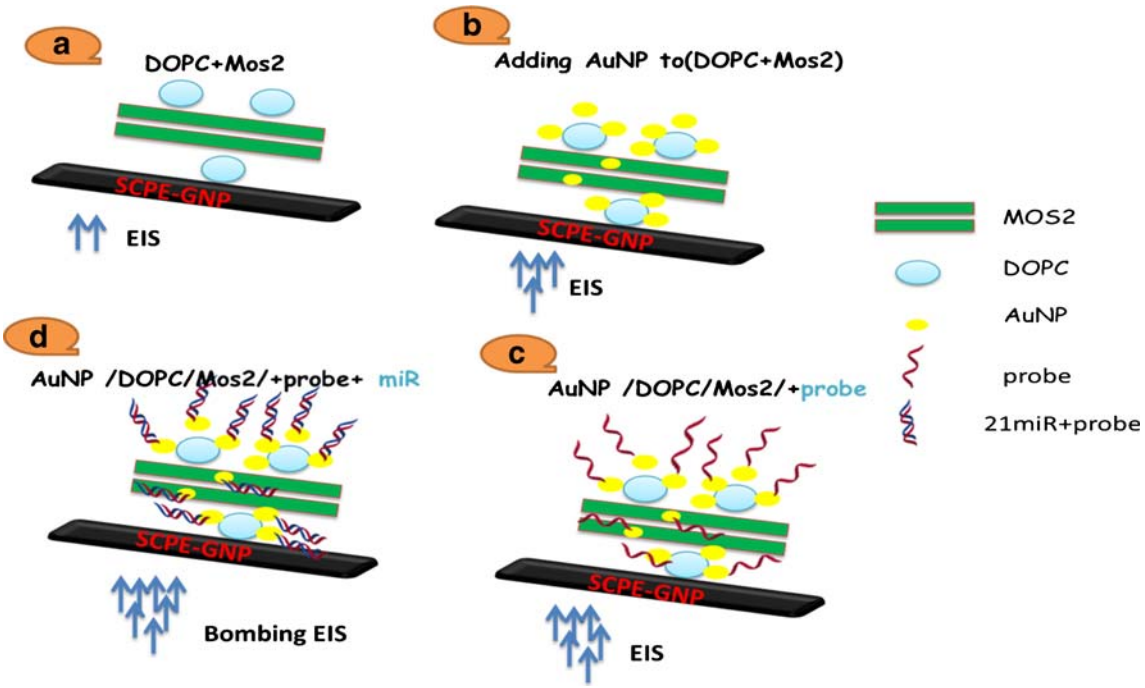

Fig. 2 The sequential detection of miR-21 by the DOPC-MoS_2/AuNP. (**A**) A self-assembled of DOPC-MoS_2 in the SCPE-GNP. (**B**) Incubation of sensor with AuNP caused an increase in the resistance measured by EIS. (**C**) Adding probe increase more resistance range. (**D**) Hybridization of mir-124a with probe increases most resistance

structure of MoS_2 nanosheets (as control image) with crumpled and wrinkled structure further confirms that the exfoliated nanomaterials exist as thin sheets with sizes varying from 200 nm to several micrometers (Fig. 3a (A)). The AFM image of the DOPC-MoS_2 hybrid surface shows the smooth surfaces. The DOPC liposomes were examined to have 70–80 nm size which they placed on and bottom the MoS_2 (Fig. 3a (B)). In the first step of adding AuNP on the surface of electrode, it was clear that the DOPC-AuNP was first formed due to direct dropping of AuNP (Fig. 3a (C)). Many researches have done simple attachment of AuNP with different types of liposome [21, 22]. On the other hand, the AFM image shows that there is not any connection of AuNP with MoS_2 (Fig. 3a (C)). It can demonstrate that DOPC-AuNP was first formed on the electrode with showing higher size of DOPC (100–110 nm). In the following, Fig. 3a (D) shows that the MoS_2-AuNP through decorated AuNP on the MoS_2 was formed. With the addition of the AuNP in situ, it has grown with an average diameter of 20 nm and homogeneously dispersed on the surface of MoS_2 nanosheets (Fig. 3a (D)). Moreover, EDS analysis was done to show the synthesis of MoS_2-AuNP. As shown in Fig. S2A (see the ESM), Au element appeared in the composition of MoS_2-AuNP compared to MoS_2, indicating the successful synthesis of MoS_2-AuNP. Further, we used as UV-vis spectrum in Fig. S3 (see the ESM) to show the DOPC and DOPC-MoS_2 and DOPC-MoS_2/AuNP suspensions. The DOPC shows one absorption peaks at around 230 nm (curve a, A), and the MoS_2 demonstrated

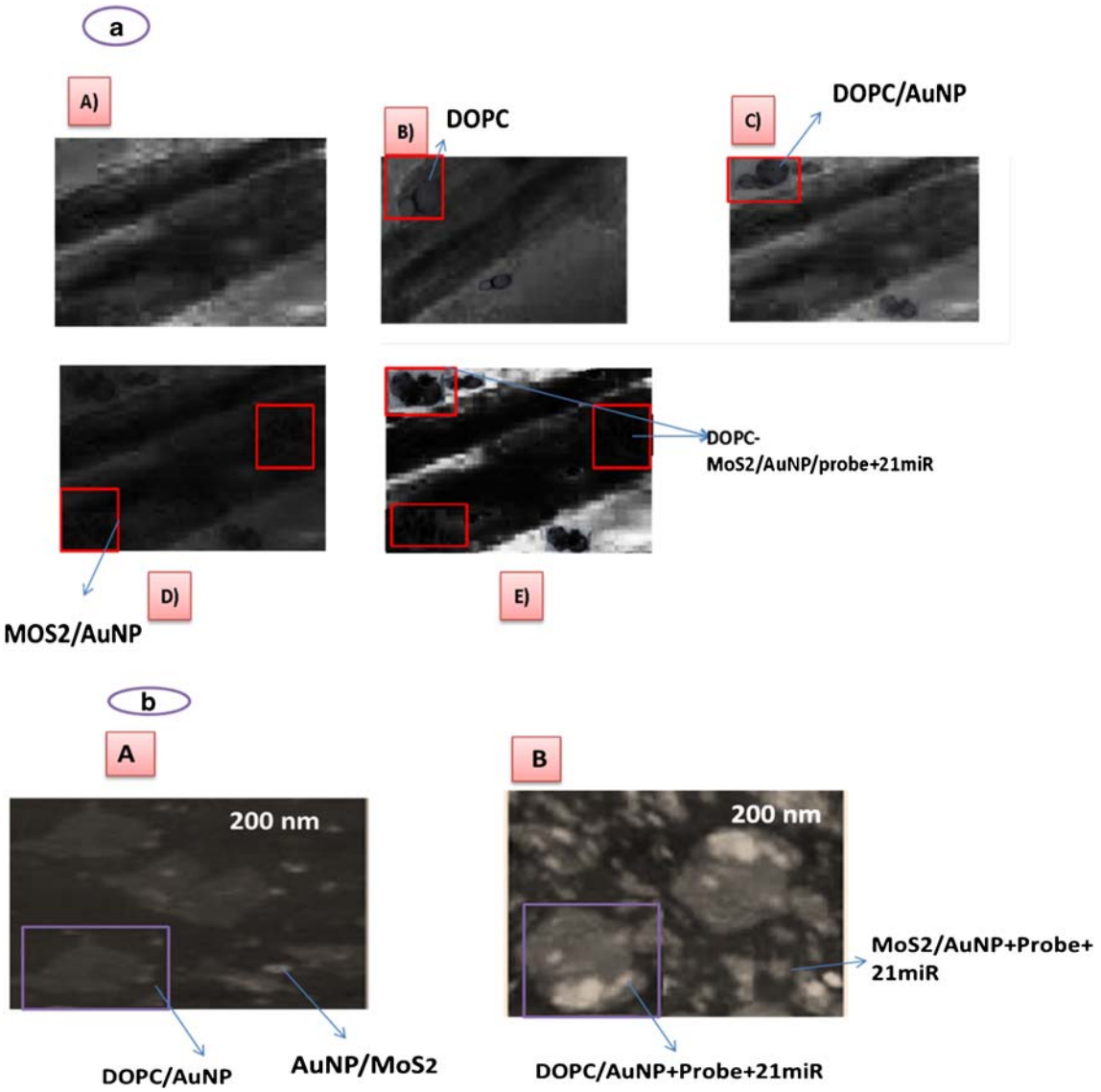

Fig. 3 **a** AFM and **b** TEM images of DOPC-MoS_2/AuNP miR sandwiching as an example. (A) M_OS_2 bed in AFM image (as control image). (B) DOPC-MoS_2 AFM image. (C) DOPC-AuNP/MoS_2 in AFM image at the early stages of adding of AuNP. (D) (DOPC-MoS_2) AuNP in AFM image at the end stage of adding of AuNP. (E) DOPC-MoS_2/AuNP/probe + miR-21 in AFM image. **b** (A) DOPC-MoS_2/AuNP in TEM image. (B) DOPC-MoS_2/AuNP/probe + miR-21 in TEM image

three absorption peaks at around 470, 610, and 670 nm (curve a, B), which was consistent with the reported results [29, 30]. In the earlier adding of AuNP, there was an obvious peak for DOPC/AuNP-MoS_2 at ~ 560 nm which AuNP added to DOPC (curve c, ESM Fig. S2B). In the following, when the AuNP was decorated on MoS_2 nanosheets by microwave-assisted one-pot method, there was an obvious peak for AuNP at 540 nm (curve d, ESM Fig. S2B) due to the amount of Au loading in MoS_2 suspension. Figure 3a (E), shows the image of DOPC at higher magnification in the DOPC-MoS_2/AuNP/probe + miR-21 stage than DOPC in the DOPC-MoS_2/AuNP stage. On the other hand, DOPC-MoS_2/AuNP/ probe + miR-21 create a smoother surface than DOPC-MoS_2 hybrid. There are dots in Fig. 3a (C–E) which belong to AuNP with the attachment of the MoS2 and DOPC with different sizes. It is clear that there were larger sizes at the DOP-MoS_2/AuNP/probe + miR-21 stage due to attachment of the probe + miR-21 with AuNP-attached DOPC and MoS_2. To illustrate the best interaction of component in different stages, the TEM images have been used, too. Figure 3b (D) shows the TEM images of the modified DOPC-MoS_2 on the carbon-coated copper grid acquired at different time intervals when AuNP (in the form of dots) was connected to the both of them. In the following, with the addition of probe +miR-21, the dots have been shown with larger size in the MoS_2 than in the MoS2/AuNP due to the addition of probe + miR-21, Fig. 3b (E). On the other hand, it is quite evident to increase in the size in the DOPC liposome when probe + miR-21 was added to AuNP-attached DOPC compared to DOPC/AuNP mode without it.

Identification of control tests (sensitivity and specificity) for sensing miR-21 on the DOPC-MoS_2/AuNP sensor

As described, the increased accumulation of the negative charge density was shown at the solution interface with the increasing electrostatic repulsion between the negatively charged hybrids of probe + miR-21 and $[Fe(CN)_6]^{-3/-4}$ probe. Molecular crowding showed decreased peak currents (DPV) and increased R_{CT} for the complementary hybridized surface. In Fig. 4A, the hybridization with buffer as a negative control of miR-21 showed a 32% increase in the j value (12.7247 μA cm^{-2}) and attachment with non-complementary (target II) of miR-21 caused a 19.8% increase in the j value (11.56 μA cm^{-2}), respectively. DPV images of hybridization with mismatch RNA of probe + miR-21 showed an 18.9% and 16.9% increase in the j value (1078.2 μA cm^{-2}). Recent studies have shown higher effect of electrochemical reactions of AuNP when it is added to liposome bed (DOTAB, DOPE) [18, 25]. In this research, we compared MoS_2 electrochemical effect when it is added to liposome bed (DOPC) related to DOPC-AuNP hybrid. DPV tests of the DOPC/AuNP and DOPC/MoS_2 electrodes showed an enhanced electrochemical reactivity of DOPC/MoS_2 compared with DOPC/AuNP as shown in Fig. 4B. Peak currents showed 15.9 and 17.3 μA for DOPC/MoS_2 and DOPC/AuNP, respectively. The best reason for these results can be the large surface area of MoS_2 with high conductivity which can provide large surface-to-volume ratio on the DOPC bed. So, it can cover more pores of spherical liposome and increase the higher electrochemical reaction with the electrode and $[Fe(CN)_6]^{-3/-4}$ probe than the AuNP/DOPC bed. In our other research, we changed the type of liposome and evaluated the effect of electrochemical reactions with AuNP and MoS2. According to the previous studies, the differences in electrochemical behavior between the interactions of positively charged liposomes (DOPE-DOTAP/DOPE) with the different structures were investigated. Results showed that there were the best electrochemical interactions of the AuNP with the DOTAP/DOPE liposomes due to the coating of more pores in the surface of the electrode [21, 27]. In this study, we use DOPE liposomes, which have the same positive charged as phosphatidylethanolamine to compare DOPC with positive phosphatidylcholine. Peak currents of 16.3 and 18.1 μA for DOPE/MoS_2 and DOPE/AuNP, respectively, are shown (Fig. 4B). DOPE like DOPC has more electrochemical reactions with MoS_2 than AuNP. The results of study indicated that the rate of electrochemical behaviors were for DOPC/MoS_2 > DOPE/MoS_2 > DOPC/AuNP > DOPE/AuNP. Interactions of van der Waals force with MoS_2 and DOPC can probably be an important cause for the higher resistance than DOPE/MoS_2. We do not know what it is the interaction between DOPE and MoS_2. However, what is quite evident is that there was weaker force than the van der Waals force between DOPC and MoS_2. Therefore, future studies should investigate what the interaction between DOPE and MoS_2. On the other hand, it is clearly evident that DOPE/MoS_2 had also higher resistance than DOPE/AuNP due to higher surface-to-volume ratio of MoS_2. An interesting result in this study was the higher sensitivity of the DOPC-MoS_2/AuNP hybrid to sensing miR-21. As seen in the results in Fig. 5A, the j value increases linearly with the increasing concentration of miR-21 ranging from 100 fM to 1 aM. A regression equation of $y = 13.876x + 21.548$ ($R^2 = 0.976$) was obtained, where y is the j value in μA cm^{-2} and x is the logarithmic concentration of miR-21 in aM. As shown in Fig. 5B, the relative standard deviation (RSD) values were between 7 and 7.6% and the limit of detection (LOD) was 10 aM. It was done from 3(Sb/m), where Sb is the standard deviation of the measurement signal for the blank and m is the slope of the analytical curve in the linear region. This can be due to the more sites of AuNP connected to the probe. So, they have greatly enhanced the capability of miR-21 detection on the DOPC-MoS_2/AuNP bed. This limit of detection is two orders more than the other liposomal sensor without MoS_2 [21, 27]. To distinguish between the sensitivity of miR-21 about this modified sensor (DOPC-MoS_2/AuNP),

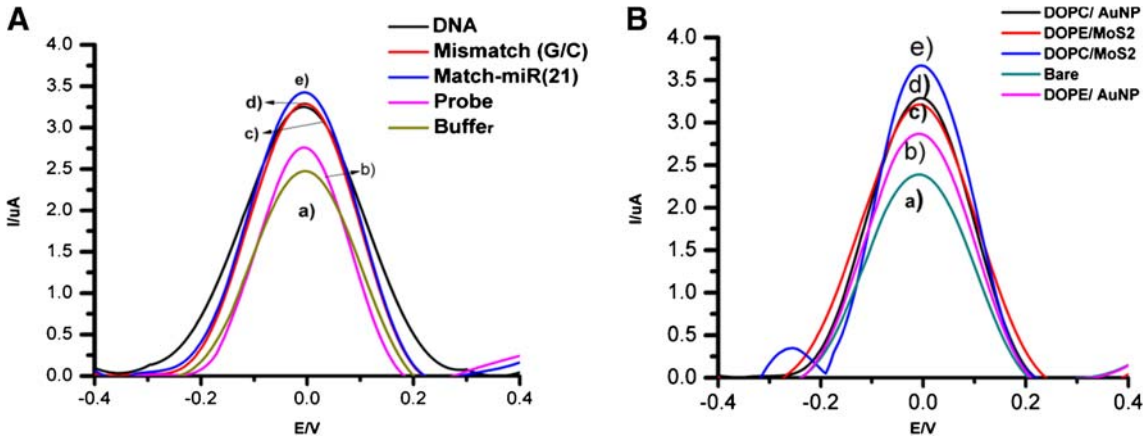

Fig. 4 **A**, **B** Control tests to check the sandwiched material on the sensor. **A** DPV obtained for detection mismatch base (DNA) and non-complementary RNA for sensing miR-21. **B** DPV obtained to detect the power of the electrochemical reaction based on changing the material (DOPE related to DOPC) and (MoS_2 related to AuNP)

we compared the results with the sensitivity of miR-21 in the presence of DOPC-AuNP, alone. As seen in Fig. 5C, the *j* value increases linearly with increasing concentration of miR-21 ranging from 1 fM to 100 pM. A regression equation of $y = 11.457x + 11.548$ ($R^2 = 0.976$) was obtained, where *y* is the *j* value in μA cm^{-2} and *x* is the logarithmic concentration of miR-21 in fM. As shown in Fig. 4D, the relative standard deviation (RSD) values were between 7 and 7.6% and the

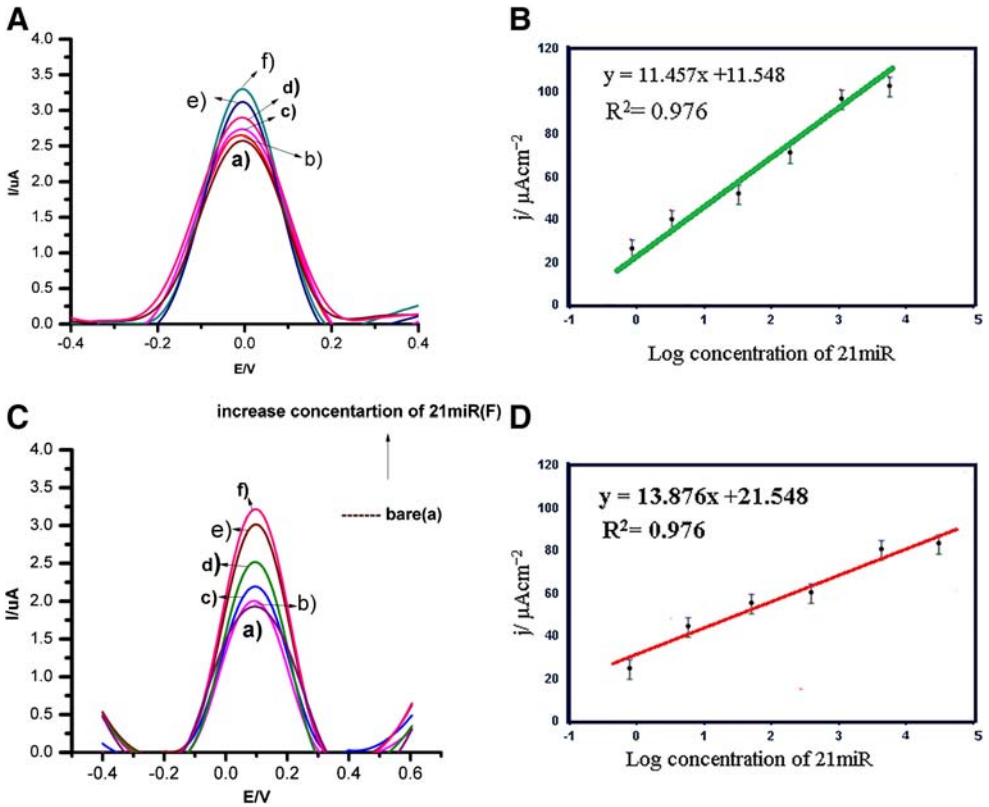

Fig. 5 The performance of the sensor for determining the concentration of target measured using DPV measured at a scan rate 50 mV s^{-1} in phosphate buffer (pH 7.4). **A** DPV of the DOPC-MoS_2/AuNP sensor obtained using (a) 10 aM, (b) 100 aM, (c) 500 aM (d), 10 fM (e), 1 fM, and (f) 100 fM of miR-21 in the incubation buffer. **B** A calibration plot of the current density vs log concentration of miR-21 in DOPC-AuNP. **C** DPV of the DOPC-AuNP sensor obtained using (a) 1 fM, (b) 10 fM, (c) 100 fM, (d) 500 fM, (e) 1 pM, and (f) 10 pM of miR-21 in the incubation buffer. **D** A calibration plot of the current density vs log concentration of miR-21 in DOPC/AuNP

Table 1 Comparison of sensitivity of the different of liposomal substrates in electrochemical biosensor

Lipid–platforms	Lipid	Bed	Specific	Sensitive	Reproducibility	Ref
Sandwiching DOTAP liposome in gold nanoparticle on solid transducer for electrochemical ultrasensitive DNA detection and transfection	DOTAP	DOTAP-AuNP	Medium	1 pM	Low	[10]
Gold surface supported spherical liposome–gold nanoparticle nanohybrid for label-free DNA sensing	DOPE	DOPE-MPA	Medium	1 fM	Low	[12]
Supported binary liposome vesicle-gold nanoparticle for enhanced label-free DNA and protein sensing	DOPE-DOTAP	DOPE-DOTAP-AuNP	Medium	1×10^{-14} M	Medium	[26]
Sequential or multiplex electrochemical detection of miRs based on the p19 function relative to three sandwiches of different structural hybrids on the liposomal sensor	DOPE-DOTAP	DOPE-DOTAP/P19	Medium	0.1 fM	High	[18]
Exosomal bed by using multicovalent attachment p19	Exosome	Exosome-p19	Medium	1 aM	High	[25]
Attomole DNA electrochemical sensor for the detection of *Escherichia coli* O157	DPPC, cholesterol, DPPG, and PE-MCC	Liposome AuNP	Low	0.1 pM	Low	[31]
Sandwiched three probes on one electrode	DOTAP-DOPE	DOTAP-DOPE/AuNP	Medium	0.5 fM	Medium	[32]
Designing of DOPC-MoS2/AuNP hybrid as organic bed with the bombing amplifier for detection of miR in electrochemical biosensor	DOPC	DOPC-MoS2/AuNP	Medium	1 aM	High	This study

limit of detection (LOD) was 10 fM. So, results showed that there were higher capabilities of DOPC-MoS_2/AuNP sensor than DOPC-MoS_2/AuNP sensor to detect miR-21. In Table 1, the sensitivity of miR based on the different types of the liposome has been shown. Generally, we show the increased effect of MoS_2 on the sensitivity of the liposomal surface compared to another controls in this study. We attribute to the enhanced performance of DOPC-MoS_2/AuNP sensor for the large surface-to-volume ratio between the DOPC nanostructure with high conductivity and a large surface of MoS_2.

Stability and reproducibility results for the DOPC-MoS2/AuNP sensor

We evaluated the stability and repeatability of DOPC-MoS_2/AuNP sensor. The stability of this sensor was confirmed after 25 cycles by DPV curves in PBS (phosphate-buffered saline) buffer; the electrode was stored in the 4 °C refrigerator for 20 days. No obvious change was seen in the peak current (Fig. 6B). The reproducibility was examined by testing five different electrodes in PBS buffer based on independent fabrication for their current response. From results shown in Fig. 6A,

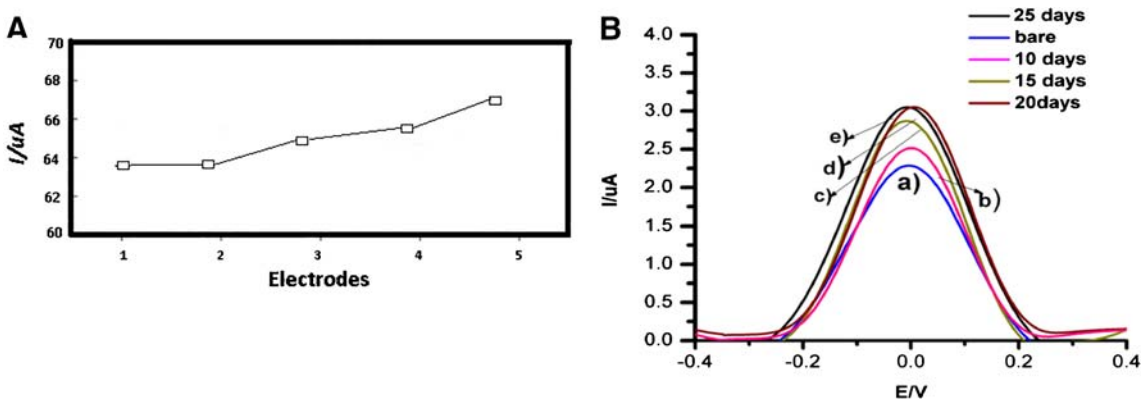

Fig. 6 **A** Reproducibility image of DPV tests in DOPC-MoS_2/AuNP bed with five electrodes. These tests were done simultaneously on the separates electrodes. **B** DPV behaviors of stability of DOPC-MoS_2/AuNP sensors in different days. DPV does not show to change

the biosensor is highly reproducible. To obtain the best analytical performance for miR detection, experimental parameters such as probe-miR-21 hybridization time and pH value were optimized. The current response increased with probe-miR-21 hybridization and reached plateaus at 60 min (ESM Fig. S3a). Thus, the optimum probe-miR-21 hybridization time was considered as 60 min. miR-21 detection and electrochemical signal are both related to pH. From Fig. S3b (see the ESM), the current response gradually increased from pH 5.5 to pH 8 and then decreased. Thus, the electrochemical sensor was performed in the pH 7.5 reaction solution.

Conclusion

Low concentration of circulating microRNA has been a challenge in the diagnostic tests [30, 33]. Studies of the liposomal sensors have been reported as the biocompatible diagnostic and therapeutic tools for miRs [21, 22]. However, the liposomal sensors had a challenge in the diagnostic test because of low sensitivity [32, 34]. In this study, a sensitive design was developed based on the DOPC-MoS_2-AuNP bed to prompt the sensitivity of liposomal sensor for detection of miRs using inexpensive fabrication methods and biocompatible materials. This study showed a simple mechanism where the higher amount of probes precisely increase the electrochemical reactivity of $[Fe(CN)_6]^{-3/-4}$ probe through the potential composition of DOPC and MoS_2 which are connected to AuNP. On the other hand, the porous nanostructures of MoS_2 and large surface areas of DOPC enhanced the interactive sites between $[Fe(CN)_6]^{-3/-4}$ probe and duplex of nucleic acid in the DOPC-MoS_2-AuNP bed, too. Therefore, the combinations of DOPC-MoS_2/AuNP hybrid have led to providing more interactions for the probe and miR-21, which increase the high sensitivity of the sensor. This sensor exhibited an excellent sensitivity, stability and reproducibility, and selectivity, suggesting a novel candidate to detect the miR in the point of care test. Further, the mechanism and fabrication method offer a novel approach for the development of liposomal biosensors with MoS_2 and large-scale manufacturing. However, in future studies, more research should be done in real-time samples and in vivo studies and in using the other 2D nanomaterials with biocompatible materials in point of care researches.

Acknowledgments The authors thank the Iran Nanotechnology Initiative Council and Prof. Seyed Mahdi Rezayat, Physics Laboratory in Tarbiat Modares University for supporting this project.

Compliance with ethical standards

Conflict of interest The authors declare that they have no conflict of interests.

References

1. Bell J. Predicting disease using genomics. Nature. 2004;429:453–6.
2. Elham G, Ganji S, Massey Z, Jamiallahmadi K. Relation of circulating micrornas as biomarkers in few diseases. J Clin Biomed. 2016;321:412–14.
3. Ye J, Xu M, Tian X, Cai S, Zeng S. Research advances in the detection of miRNA. J Pharm Anal. 2019;217:311–26.
4. Cheng Y, Dong L, Zhang J, Zhao Y, Li Z. Recent advances in microRNA detection. Analyst. 2018;143(8):1758–74.
5. Chandrasekaran AR, Punnoose JA, Zhou L, Dey P, Dey BK, Halvorsen K. DNA nanotechnology approaches for microRNA detection and diagnosis. Nucleic Acids Res. 2019;47(20):10489–505.
6. Johnson BN, Mutharasan R. Biosensor-based microRNA detection: techniques, design. Analyst. 2014;139:1576.
7. Han S, Liu W, Yang S, Wang R. Facile and label-free electrochemical biosensors for microRNA detection based on DNA Origami nanostructures. ACS Omega. 2019;4(6):11025–31.
8. Gillespie P, Ladame S, O'Hare D. Molecular methods in electrochemical microRNA detection. Analyst. 2019;144:114–29.
9. Shimon S, Pardeeb K, James J. Synthetic biology devices for in vitro and in vivo diagnostics. pnase. 2015;112(47):14429–35.
10. Narayanan SJ, Bhuvana M, Dharuman V. Sandwiching spherical 1, 2-dioleoyltrimethylammoniumpropane liposome in gold nanoparticle on solid transducer for electrochemical ultrasensitive DNA detection and transfection. Biosens Bioelectron. 2014;58:326–32.
11. Kilic T, Topkaya SN, Ozsoz M. A new insight into electrochemical microRNA detection. Biosens Bioelectron. 2013;48:165–71.
12. Bhuvana M, Narayanan JS, Dharuman V, Teng W, Hahn JH, Jayakumar K. Gold surface supported spherical liposome-gold nano-particle. Biosens Bioelectron. 2013;41:57–112.
13. Susana C, Pedrero M, Pingarrón JM. Electrochemical genosensors for the detection of cancer. Anal Bioanal Chem. 2014;406:27–33.
14. Zhu C-s, Zhu L, Tan D-a, Qiu X-y, Liu C-y, Xie S-s, et al. Avenues toward microRNA detection in vitro: a review of technical advances and challenges. Comput Struct Biotechnol J. 2019;17:904–16.
15. Zouari M, Campuzano S, Pingarrón J, Raouaf N. Amperometric biosensing of miRNA-21 in serum and cancer cells at nanostructured platforms using anti-DNA–RNA hybrid antibodies. ACS Omega. 2018;3:8923–31.
16. Chen C, Wang Q. Liposome-based nanosensors for biological detection. Am J Nano Appl. 2015;3(1–1):13–7.
17. Ding W, Palaiokostas M, Wang W, Orsi M. Effects of lipid composition on bilayer membranes quantified. J Phys Chem B. 2015;119:15263–74.
18. Cordeiro M, Carlos FF, Pedrosa P, Lopez A, Baptista PV. Gold nanoparticles for diagnostics: advances towards points of care. Diagnostics. 2016;6:43.
19. Ferhan AR, Ma GJ, Jackman JA, Sut TN, Cho JHPN-J. Probing the interaction of dielectric nanoparticles with supported lipid membrane coatings on nanoplasmonic arrays. Sensors. 2017;17:1484.
20. Xia M, Palaiokostas M, Wang W. Adsorption separation of acetylene and ethylene in a highly thermostable microporous metal-organic framework. Chem Sci. 2017;137:119–31.
21. Feng K, Liu J, Deng L, Yu H, Yang M. Two-dimensional nanomaterial based sensors for heavy metal ions. Microchim Acta. 2019;185(1):28.
22. Yammour G, Mohammadi H, Amine A. A highly sensitive electrochemical biosensor based on carbon black and gold nanoparticles modified pencil graphite electrode for microRNA-21 detection. Chemistry Africa. 2019;9:75–111.
23. Li Z, Jiang S, Huo Y, Liu M, Cheng Y, Zhang C, et al. Controlled-layer and large-area MoS2 encapsulated Au nanoparticle hybrids for SERs. Opt Express. 2019; 24(23):22–112.

24. Frens G, Kolloid Z. Controlled nucleation for the regulation of the particle size in monodisperse gold suspensions. Nat Phys Sci. 1973;241:20–2.
25. Ganguly A, Benson J, Papakonstantinou P. Sensitive chronocoulometric detection of miRNA at screen-printed electrodes modified by gold decorated MoS2 nanosheets. ACS Appl Bio Mater. 2018;1(4):1184–94.
26. Divya KP, Dharuman V. A novel signal-off electrochemiluminescence biosensor. Biosens Bioelectron. 2017;95:168–73.
27. Su S, Sun HF, Xu F, Yu LH, Fan CH, Wang LH. Direct electrochemistry of glucose oxidase and a biosensor for glucose based on a glass carbon electrode modified with MoS2 nanosheetsdecorated with gold nanoparticles. Microchim Acta. 2014;181:1497–503.
28. Ghazizadeh E, Hosseinkhanib S, Oskueea RK, Molaabasic F, Jaafari MR. Sequential or multiplex electrochemical detection of miRs based on the p19 function relative to three sandwiches of different structural hybrids on the liposomal sensor. Mater Sci Eng C. 2018;4931(17):33550–6.
29. Elham G, Naseri Z, Jaafarib MR, Mehdi Forozandeh M, Hosseinkhani S. A fires novel report of exosomal electrochemical sensor for sensing micro RNAs by using multi covalent attachment p19 with high sensitivity. Biosens Bioelectron. 2018;113(15):74–81.
30. Ghazizadeh E, Oskuee RK, Jaafari MR, Hosseinkhan S. Electrochemical sensor for detection of miRs based on the differential effect of competitive structures in the p19 function. Sci Rep. 2018;8:3786.
31. Liao W-C, Ho J-a A. Attomole DNA electrochemical sensor for the detection of E. coli. Anal Chem. 2009;81:2470–6.
32. Wang Y-H, He L-L, Huang K-J, Chen Y-X, Wang S-Y, Liu Z-H, et al. Recent advances in nanomaterial-based electrochemical and optical sensing platforms for microRNA assays. Analyst. 2019;144:2849–66.
33. Pankaj R, Gao Y, Ozsoz M, Mulchandani A. Electronic detection of microRNA at attomolar level with high specificity. Anal Chem. 2013;43:56–9.
34. Zouari M, Campuzano S, Pingarrón JM, Raouafinsor N. Ultrasensitive determination of microribonucleic acids in cancer cells with nanostructured-disposable electrodes using the viral protein p19 for recognition of ribonucleic acid/microribonucleic acid homoduplexes. Electrochim Acta. 2018;262:39–47.